



OPEN ACCESS

EDITED BY

Jurriaan Boon,
Netherlands Organisation for Applied
Scientific Research, Netherlands

REVIEWED BY

Zhiming Zhou,
East China University of Science and
Technology, China
Ki Bong Lee,
Korea University, South Korea
Vladimir Dikic,
Netherlands Organisation for Applied
Scientific Research, Netherlands

*CORRESPONDENCE

Peter Pfeifer,
peter.pfeifer@kit.edu

SPECIALTY SECTION

This article was submitted to Chemical
Reaction Engineering,
a section of the journal
Frontiers in Chemical Engineering

RECEIVED 21 July 2022

ACCEPTED 10 October 2022

PUBLISHED 25 October 2022

CITATION

Stadler TJ, Bender LJ and Pfeifer P
(2022), Dynamic simulation of a
compact sorption-enhanced water-gas
shift reactor.
Front. Chem. Eng. 4:1000064.
doi: 10.3389/fceng.2022.1000064

COPYRIGHT

© 2022 Stadler, Bender and Pfeifer. This
is an open-access article distributed
under the terms of the [Creative
Commons Attribution License \(CC BY\)](#).
The use, distribution or reproduction in
other forums is permitted, provided the
original author(s) and the copyright
owner(s) are credited and that the
original publication in this journal is
cited, in accordance with accepted
academic practice. No use, distribution
or reproduction is permitted which does
not comply with these terms.

Dynamic simulation of a compact sorption-enhanced water-gas shift reactor

Tabea J. Stadler, Laila J. Bender and Peter Pfeifer*

Institute for Micro Process Engineering (IMVT), Karlsruhe Institute of Technology (KIT), Karlsruhe, Germany

This work presents the dynamic simulation of a novel sorption-enhanced water-gas shift reactor used for synthesis gas production from pure CO in an e-fuels synthesis process. Due to the intended decentralized plant installation associated with fluctuating feed, process intensification and a compact reactor system is required. An optimized operating procedure was obtained by simulation-driven process design to maximize the sorbent loading and operate the process as efficient as possible. The process simulation is based on a simplified heterogeneous packed bed reactor model. The model accounts for simultaneous water-gas shift (WGS) reaction on a Cu-based catalyst and CO₂ adsorption on a K-impregnated hydrotalcite-derived mixed oxide as well as subsequent desorption. An empirical rate expression was chosen to describe the water-gas shift reaction according to experimental data at 250°C. Breakthrough experiments were performed and used to adapt kinetic adsorption (pressure: 8 bar) and desorption (pressure: 1 bar) parameters. The experimental CO₂ sorption equilibrium isotherm was fitted with the Freundlich model. The reactor model was extended to a complex hybrid system scale model for the pilot plant reactor consisting of six individually accessible reaction chambers. Cyclic operation with automatized switching time adjustment was accomplished by a finite state machine. A case study exploited the benefits of a serial process configuration of reaction chambers. It could be shown that the sorbent loading can be remarkably increased through optimized operating strategies depending on the process conditions. Hence, the development of the hybrid model marks a crucial step towards the planned pilot plant operation and control.

KEYWORDS

sorption-enhanced water-gas shift reaction, dynamic simulation, MATLAB Simulink Stateflow, experimental model validation, simulation-driven process optimization, micro-structured reactor design, high-temperature CO₂ adsorption

1 Introduction

Global CO₂ emissions unexpectedly dropped by 5.4% in 2020 due to the COVID pandemic, but pre-COVID levels have been reached again rapidly (UNEP, 2021). International aviation is among the top emitters. It released about 1 Gt CO₂ to the atmosphere in 2018 (Lee et al., 2021) and the global aviation industry expects

emissions to increase to about 1.2–1.9 Gt CO₂ in 2050 (Fleming and de Lépinay, 2019). Although these predictions were made before the pandemic, they do not lose their long-term significance, because the pandemic-related impacts are expected to be only relevant until around 2024 (IATA, 2020).

To still achieve the Paris climate goals and limit global warming to well below 1.5°C, net zero CO₂ emissions have to be reached by around 2050 (IPCC, 2018). Hence, also the aviation sector has to undergo a transition away from fossil fuels until 2050. The decarbonization of aviation is especially demanding due to extremely long technology and fleet turnover times. Therefore, it is highly likely that planes still have to be powered with hydrocarbons in the upcoming decades. Sustainable aviation fuels (SAF) as fossil fuel substitutes remain the only reasonable near- to mid-term solution.

SAF can be classified into biofuels produced from biomass, and e-fuels obtained from renewable energy, CO₂ and water. Biofuel production technologies are already available in industrial scale, but biofuel availability is limited by natural and ethical constraints. The global SAF demand in 2050 cannot be met completely by biofuels under sustainable aspects, such as protecting ecosystems and ensuring availability of land and water without competition. E-fuels production, however, is primarily limited by the cost and availability of renewable energy.

Established e-fuels process routes include H₂ production *via* water electrolysis in combination with CO generation *via* reverse water-gas shift reaction from air-captured CO₂ (Kirsch et al., 2020). Synthesis gas (CO and H₂) is then chemically converted to e-fuels *via* Fischer-Tropsch reaction and further downstream processing steps (Stadler et al., 2022a).

The Kerogreen project currently investigates a novel e-fuels process route with an advanced synthesis gas production concept (Goede, 2018; Kerogreen, 2022). Compact, decentralized plants close to renewable energy production sites are envisaged. Here, CO₂ is split into CO and O₂ in a plasmolysis unit. Pure CO partly reacts with steam to H₂ *via* water-gas shift (WGS) reaction. The by-product CO₂ is removed *in-situ* and recycled to the plasmolysis unit. The energy for the plasmolysis unit is provided by renewable sources.

For the WGS process step with simultaneous CO₂ separation, the sorption-enhanced water-gas shift (SEWGS) reaction concept was chosen. SEWGS applications were first described by Gluud et al. (1931) and have been broadly discussed for H₂ production, purification, and pre-combustion capture technologies in the past decade (Jansen et al., 2013; Petrescu et al., 2019; Sebastiani et al., 2022). The concept is based on a homogeneous mixture of solid catalyst and sorbent material in a packed bed reactor. The catalyst

enables the exothermic WGS reaction (Eq. 1) while the sorbent is capable to adsorb the produced CO₂ under the prevailing process conditions, e.g., at elevated temperature (200°C–450°C). Hence, the thermodynamic boundary conditions are shifted towards favorable H₂ generation according to LeChatelier's principle.



The most intensively discussed materials for CO₂ adsorption include calcium oxide (Wang et al., 2013), magnesium oxide (Bhagiyalakshmi et al., 2010), lithium zirconate (Iwan et al., 2009), lithium silicate (Hu et al., 2019), activated carbon (Yin et al., 2013), molecular sieves (Siriwardane et al., 2001), zeolites (Mulloth and Finn, 1998), metal organic frameworks (Millward and Yaghi, 2005), and layered double hydroxides (Rives, 2002). Hydrotalcites (HTC) belong to the latter group and change their structure during thermal treatment to a hydrotalcite-derived mixed oxide (HDMO) form, so that suitable basic properties for CO₂ adsorption under WGS conditions are revealed (León et al., 2010; van Selow et al., 2011; Salomé Macedo et al., 2021). HDMOs are frequently employed in SEWGS processes due to their stable thermal and mechanical properties, good performance in the presence of steam, high adsorption selectivity towards CO₂, relatively fast sorption kinetics, low energy requirement for regeneration, and cyclic performance (Yong et al., 2001; Soria et al., 2015). Additionally, their cheap price makes them interesting for large scale applications. The relatively low adsorption capacity of HDMOs (typically below 1 mmol g⁻¹) can be improved by means of impregnation with alkali metal ions, namely potassium, to obtain potassium-impregnated hydrotalcite-derived mixed oxides (K-HDMO) (Oliveira et al., 2008; Du et al., 2010; Lee et al., 2010; Halabi et al., 2012; Zhu et al., 2017; Faria et al., 2022). K-HDMO was chosen as CO₂ adsorption material in this work.

Various catalysts (Fe-, Ni-, Cu-based) are applied in SEWGS systems (Lee et al., 2008; Beaver et al., 2009; Li et al., 2012; Cunha et al., 2015; Moreira et al., 2016; Cunha et al., 2017). The choice of catalyst depends mainly on the intended process operating conditions as well as on the employed sorbent. Occasionally, it has been reported that specific sorbent materials can exhibit sufficient catalytic activity, so that a separate catalyst may even be omitted (van Selow et al., 2013). Promising candidates in combination with K-HDMOs are Cu-based low-temperature WGS catalysts with operating temperatures from 200°C to 300°C (Soria et al., 2019). Such a catalyst was chosen in this work.

A major challenge in sorption-enhanced processes is caused by the relatively fast sorbent saturation. To enable continuous production, the sorbent has to be regenerated at

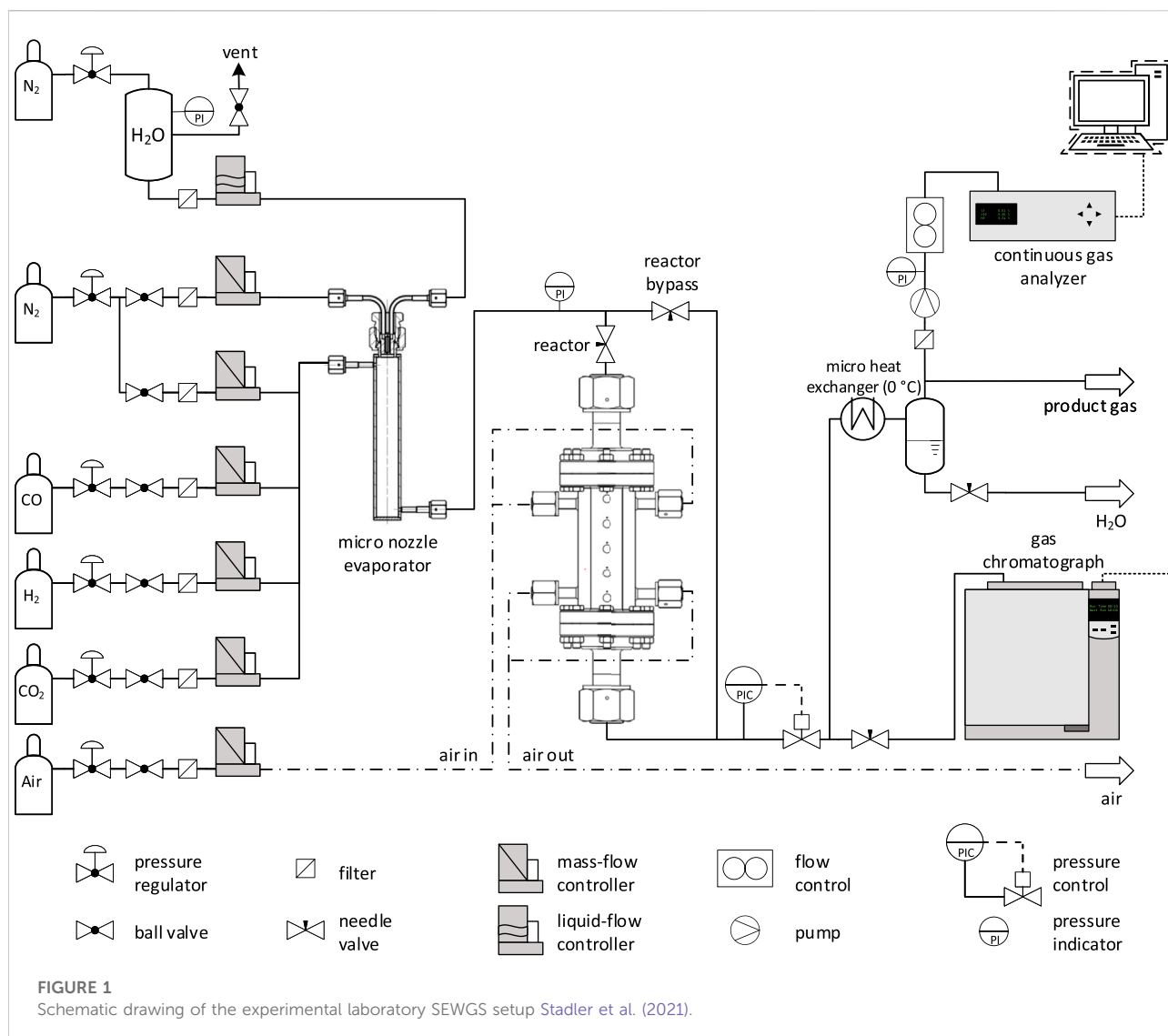
least at full saturation and cyclic operation of not less than two reactors is inevitable. A cycle may include reactive adsorption, depressurization, regeneration, and pressurization. Always (at least) one reactor is in reactive adsorption mode, while the other(s) is (are) in regeneration mode. The regeneration can either be triggered by temperature or by pressure changes. Typically, pressure swing adsorption (PSA) concepts are chosen for SEWGS systems alongside with purge gas for additional partial pressure reduction (Zhu et al., 2019). Due to the rather complex nature of a PSA-like SEWGS system with various interfering parameters, the definition of ideal operating conditions of the overall setup with multiple reactors can be challenging (Choi et al., 2003; Zheng et al., 2014). Modeling and simulation tools provide a time- and resource-efficient way to investigate a variety of influencing parameters that might be difficult to observe on a purely experimental basis in complex reaction systems. Therefore, advanced system scale models are needed to determine optimum (cyclic) operating strategies and ensure enhanced overall process performance and efficiency. System scale models are based on reactor and particle scale models to simulate reactive adsorption and subsequent regeneration.

Concerning reactor and particle scale models, significant effort was put on modeling the sorption behavior on K-HDMO under real working conditions, e.g., elevated temperature and pressure or in the presence of steam. Reactor as well as kinetic models are available in great depth. Recently, Martins et al. successfully modelled CO₂ capture from flue gas on K-HDMO at 623 K and 134 kPa in dry and wet conditions (Martins et al., 2022). They applied a bi-Langmuir equilibrium expression to consider CO₂ adsorption on two different sites and Elovich-type equations accounting for the heterogeneous adsorption/desorption activation energy. Coenen et al. (2019) intensively investigated the sorption mechanisms and kinetics of H₂O and CO₂ as well as the interactions of both components on K-HDMO. Their model includes three adsorption sites: two weaker chemisorption sites for H₂O and CO₂, respectively, and one exchange site for both gases. They concluded that the presence of steam remarkably influences the desorption behavior by means of exchanging CO₂ on the exchange site. Karagöz et al. (2019) developed a multi-scale process model with a Langmuir adsorption isotherm to quantify the catalyst and adsorbent effectiveness factors and stated a rapid convergence to a long-term cyclic solution. Likewise, a variety of kinetic expressions is given in literature for the WGS reaction rate on low-temperature Cu-based catalysts. Some suggestions include mechanistic aspects derived from redox (Uchida et al., 1967; Ovesen et al., 1996) or Langmuir-Hinshelwood-type models (Amadeo and Laborde, 1995), while others are purely

empiric (Ovesen et al., 1996; Choi and Stenger, 2003; Koryabkina et al., 2003). A comprehensive overview of WGS reaction models and proposed mechanisms is given by Smirniotis (2015).

Concerning system scale models, interesting concepts for multi-column PSA systems were published. For example, Boon et al. (2014) and Boon et al. (2015) presented the simulation of a complete SEWGS cycle consisting of eleven steps in a nine-column system. The simulation is based on their single column model and was used to establish an enhanced cycle design (Boon et al., 2014; Boon et al., 2015). Another multi-train model was developed by Najmi et al. (2016). Their system consists of eight parallel reactors and shows the influence of rinse and purge steam loads on CO₂ purity for predefined cycle times. The authors concluded that cycle times should be adjusted depending on the feed gas composition to maintain the target performance. More recently, Sebastiani et al. (2021) demonstrated a six reactor SEWGS model and validated it with single column and multi-column experiments with simulated blast furnace gas. Here, always one column is calculated, while the interacting column states are stored in a database for use upon requirement (Sebastiani et al., 2021).

So far, less attention has been paid to overall SEWGS modeling and practical operational concepts in small-sized apparatus under intensified process conditions. Therefore, we herein present the complete dynamic simulation of our compact pilot plant SEWGS reactor which was manufactured in the frame of the Kerogreen project. This diffusion-bonded reactor was designed for decentralized plant installation. It enables continuous cyclic operation in six packed bed reaction chambers, each with a separate in- and outlet. Due to space constraints that arise from the modular container-sized setup, the amount of available sorbent for CO₂ separation is very limited. For that reason, a carefully chosen operating strategy derived from simulation-driven process design is of utmost importance to increase the process' overall efficiency. A simplified mathematical description with experimentally determined kinetic parameters was used to model combined reaction and adsorption as well as consecutive desorption. The model accounts for mass transfer limited sorption kinetics, nonlinear adsorption equilibrium (Freundlich model), and empirical WGS reaction kinetics. It was extended for simulating the full pilot plant reactor on system scale. An elaborated graphical simulation approach in MATLAB Simulink was established to enable automated switching between reactive adsorption and regeneration in all six reaction chambers simultaneously. The hybrid system consisting of continuous states (reaction chamber conditions) and discrete states (valve positions) is controlled with a finite state machine in MATLAB Stateflow. This novel approach is capable to work without predefined switching times: switches from, e.g., reactive adsorption to regeneration occur



automatically based on the outlet CO_2 concentration to ensure constant product purity. A case study including different design configurations and process conditions was performed to identify optimum operating strategies regarding sorbent loading and process efficiency.

2 Materials and methods

2.1 Catalyst and sorbent

Commercial $\text{Cu}/\text{ZnO}/\text{Al}_2\text{O}_3$ WGS catalyst pellets were crushed and sieved to obtain particles with diameters from $100\ \mu\text{m}$ to $300\ \mu\text{m}$. Catalyst reduction took place *in-situ* under 3% H_2 in N_2 flow (up to 240°C), followed by pure H_2 flow from 240°C to 250°C .

K-HDMO served as CO_2 sorbent under WGS conditions. It was obtained through impregnation and calcination of Pural MG70 (Sasol GmbH, Germany), a HTC with $\text{Al}_2\text{O}_3:\text{MgO} = 30:70$. Pural MG70 was loaded with 20 wt% potassium to form potassium-impregnated HTC (K-HTC) by means of incipient wetness impregnation with potassium carbonate (K_2CO_3 , $\geq 99\%$, Sigma-Aldrich, United States). K-HTC was calcined *ex-situ* at 400°C in N_2 atmosphere for 10 h to K-HDMO. K-HDMO particles were crushed and sieved to keep the diameter range between $100\ \mu\text{m}$ and $300\ \mu\text{m}$.

2.2 CO_2 sorption isotherm

The physico-chemical characterization of K-HDMO in terms of a CO_2 sorption equilibrium isotherm was performed under

dry conditions with a 3Flex Surface Characterization instrument (Micromeritics Instrument Corporation, United States). Calcined and outgassed samples (~0.2 g) were exposed to pulses of analysis gas (CO₂) at 250°C (equilibration interval 20 s).

2.3 Experimental setup

Catalyst activity as well as breakthrough experiments were performed in the laboratory setup depicted in Figure 1. The results were used to estimate the model parameters introduced in Section 2.6. The gases N₂, CO, CO₂ and H₂ were fed into the system by calibrated mass flow controllers (Brooks Instrument, United States). Precise and pulsation-free steam supply was realized with a liquid flow controller (Brooks Instrument, United States) in combination with an electrically heated micro nozzle evaporator (manufactured inhouse). Unwanted condensation in the tubes was prevented by electrical heatings. All gases entered the stainless steel two-slit packed bed microchannel reactor (PBMR, manufactured inhouse), which was filled with catalyst and/ or sorbent particles, respectively. Isothermal reaction conditions in both reaction slits (each 2 mm × 50 mm × 100 mm) were ensured by five programmable electrical heating cartridges controlled by type K thermocouples, and tempering air-flow in adjacent microchannels. The reaction temperature was monitored continuously by additional type K thermocouples in the packed bed. The PBMR could optionally be bypassed for feed gas analysis. An automated valve (Flowserve, United States) regulated the system pressure. The steady-state wet gas composition was analyzed in a gas chromatograph (GC, Agilent 7890A, Agilent Technologies, United States) equipped with two columns (HP-Plot/Q and HP-Molsieve/5A, Agilent Technologies, United States) and two detectors (TCD and FID). N₂ served as internal standard and Ar as carrier gas. The CO, CO₂ and H₂ volume fractions in the dry effluent were continuously recorded in a process gas analyzer (PGA, X-STREAM Enhanced, Emerson, United States). CO and CO₂ were monitored by infrared-based detectors, and H₂ by a TCD. H₂O was removed from the gas flow in a micro heat exchanger (manufactured inhouse) in countercurrent flow with a cooling liquid (0°C). Both analyzers, GC and PGA, measured the respective gases within 1% of accuracy between each other. Further information related to the experimental setup can be found in (Stadler et al., 2021).

2.4 Water-gas shift catalyst activity experiments

For the catalyst activity tests, Cu/ZnO/Al₂O₃ particles were sufficiently diluted with silicon carbide (SiC, 100 μm–300 μm, ESK-SIC GmbH, Germany) and filled in the first quarter of the

PBMR reactor slits. The catalyst mass accounted for 0.50 g. The remaining space of the reactor slits was filled with pure SiC. This arrangement was chosen due to comparability with subsequent experiments and resulted from preliminary studies (Stadler et al., 2021). The feed gas flow rate was kept constant at 2,000 ml min⁻¹. The CO volume fraction was 0.1 and the steam content was varied to achieve Steam-to-Gas ratios between 0.5 and 4.5 (Eq. 2) balanced in N₂.

$$S/G = \frac{\dot{n}_{\text{H}_2\text{O,feed}}}{\dot{n}_{\text{CO,feed}}} \quad (2)$$

The reaction pressure was kept constant at 8 bar. The reaction temperatures were set to 225°C, 250°C, and 275°C, respectively. The temperature gradient in the catalyst bed was always kept below 1 K, hence isothermal conditions could be assumed.

GC measurements of feed and product gas compositions revealed carbon balances within 2% of closure, and no byproduct formation was detected. Preliminary tests with SiC filling without catalyst did not reveal blank activity. The steady-state conversion of CO was determined according to Eq. 3.

$$X_{\text{CO}} = \frac{\dot{n}_{\text{CO,feed}} - \dot{n}_{\text{CO}}}{\dot{n}_{\text{CO,feed}}} \quad (3)$$

2.5 CO₂ breakthrough experiments

The K-HDMO stability and cyclic working capacity was tested in typical breakthrough experiments with and without WGS catalyst under PSA conditions. Blank experiments with inert SiC particles of identical size (100 μm–300 μm, ESK-SIC GmbH, Germany) were used to determine the residence time distribution in the reactor, tubes, fittings and components. Preliminary tests without catalyst (K-HDMO sorbent only) ensured that the sorbent was not catalytically active for the WGS reaction at 8 bar and 250°C, as neither products nor byproducts of any kind were detected in the effluent.

In the first series of experiments, a pure K-HDMO filling (9.70 g) was packed into the PBMR for PSA breakthrough experiments. The adsorption step was investigated with a feed flow consisting of various compositions of CO, CO₂, H₂, and H₂O balanced in N₂. The step duration was 15 min at 8 bar and 250°C. CO and H₂ were fed for comparison with CO₂.

The second series of experiments was performed with a catalyst-sorbent-mixture PBMR filling. The first quarter of the reaction slits was packed with a homogeneous mixture of 0.51 g Cu/ZnO/Al₂O₃ catalyst and K-HDMO sorbent. The remaining space of the slits was packed with pure K-HDMO. The total sorbent mass was 9.35 g. Experimental reasons were responsible for minor deviations in the total packed bed filling weight of the two series. The reactive adsorption feed flow was varied regarding the compositions of CO and H₂O balanced in N₂. The duration of

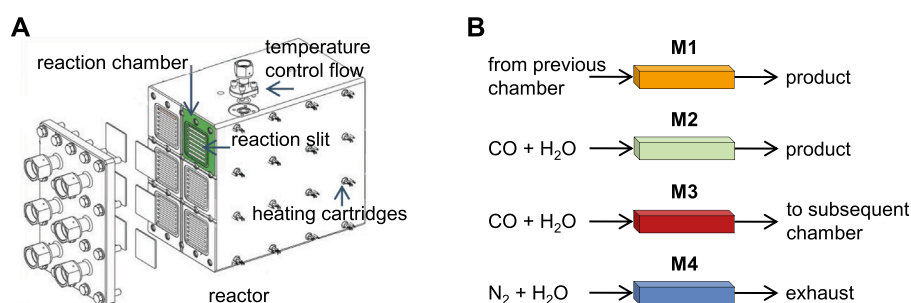


FIGURE 2

(A) Compact SEWGS pilot plant reactor with six individually fed reaction chambers, each consisting of seven rectangular slits. Microchannels and heating cartridges enable advanced temperature control for isothermal operation in the slits. Uniform gas distribution in the slits is realized by means of sintered metal plates. (B) Pilot plant reactor operation modes. M2 stands for reactive adsorption with fresh feed, and M4 for regeneration with purge flow. M1 and M3 (both reactive adsorption) occur only in serial configuration, when the outlet of one reaction chamber is optionally connected to the inlet of the subsequent reaction chamber Stadler et al. (2022b).

the reactive adsorption step was always 15 min at 8 bar and 250°C.

In both experimental series, the regeneration step was performed at 1 bar, 250°C, and lasted for 40 min. The regeneration purge gas consisted always of 40% H₂O and 60% N₂.

A LabVIEW process control program (National Instruments, United States) enabled fully automated reproducible PSA operation. All experiments were repeated with at least five and maximum 70 cycles.

2.6 Sorption-enhanced water-gas shift process model

A hybrid dynamic reactor model was developed to describe simultaneous reaction and adsorption, as well as consecutive desorption on a homogeneous catalyst-sorbent-mixture. The model is capable to automatically compute and adjust cyclic PSA switching times during runtime according to a defined threshold. This threshold can, for example, be a defined CO₂ concentration in the product flow.

The model aims to predict and plan the operation of the pilot plant reactor depicted in Figure 2A. The pilot plant reactor is basically an extended version of the laboratory-scale two-slit PBMR. It consists of six parallel reaction chambers, each with a separate in- and outlet, merged in one diffusion-bonded apparatus (manufactured inhouse). For continuous H₂ production in cyclic operation, at least one reaction chamber must be in reactive adsorption mode. Subsequent chambers can optionally be interconnected in series to maximize sorbent loading, hence, increase the time span of reactive adsorption. An overview of operation modes for the pilot plant reactor is given in Figure 2B. In serial configuration, M1-4 take place, while in single stage configuration (without interconnected chambers) only

M2 and M4 occur. In the real pilot plant as well as in the model, the switch between different modes is realized by means of discrete valve positions.

2.6.1 Conservation equations in bulk and particle phase

A simplified set of differential algebraic equations was used to describe WGS reaction and CO₂ adsorption as well as desorption in a packed bed reactor model. The homogeneous mixture of identically sized catalyst and sorbent particles was assumed as one phase. Time- and space (axially) resolved mole balances for bulk and particle phase are given in Table 1.

Internal mass transfer limitations were considered (according to Weisz-Prater-criterion) with a linear driving force (LDF) model (in line with Glueckauf-criterion), while external limitations could be neglected (proven by Maers-criterion). The initial conditions for the first step represented a fresh sorbent, while all subsequent PSA steps based on the conditions at the end of the previous step. Dirichlet boundary conditions arising from the feed flow were applied at the inlet, and Neumann boundary conditions at the outlet of each reaction chamber. Negligible pressure drop as well as the absence of gradients rectangular to flow direction could be assumed owing to the technical properties of the reactor. Isothermal conditions in the slits were realized by an advanced temperature control system: electrical heating cartridges in combination with adjacent tempering channels, where purge gas is fed through, enable excellent heat transfer.

2.6.2 Reaction and adsorption kinetics

A power law kinetic expression in combination with Arrhenius' equation (Eq. 4) was used to describe the experimental observations for the WGS reaction rate. This type of empirical expression is frequently found in literature for resembling catalysts (Smirniotis, 2015). The reaction

equilibrium constant is a function of temperature and was calculated with the well-established correlation given in Eq. 5 (Moe, 1962).

$$r_{WGS} = k_{co} \cdot \exp\left(-\frac{E_a}{R \cdot T}\right) \cdot \left(p_{CO} \cdot p_{H_2O} - \frac{p_{CO_2} \cdot p_{H_2}}{K_{eq}}\right) \quad (4)$$

$$K_{eq} = \exp\left(\frac{4577.8}{T} - 4.33\right) \quad (5)$$

The equilibrium-based ad- and desorption of CO₂ on K-HDMO surface was modelled with Eqs 6, 7, respectively (Zhu et al., 2017; Coenen et al., 2019; Martins et al., 2022).

$$a_{ads,CO_2} = k_{ads} \cdot (q_{CO_2}^{eq} - q_{CO_2}) \quad (6)$$

$$a_{des,CO_2} = k_{des} \cdot (q_{CO_2}^{eq} - q_{CO_2}) \quad (7)$$

The adsorption rate coefficient was assumed to be a function of temperature and can therefore be fitted directly. The desorption rate coefficient was described by an Arrhenius-type expression (Eq. 8). Due to the heterogeneity of the surface, an Elovich-type equation was employed to describe the activation energy of desorption (Eq. 9) (Ho, 2006). The number of fitted parameters was reduced by simplifying Eqs 8–10 (Coenen et al., 2019).

$$k_{des} = k_{des}^0 \cdot \exp\left(-\frac{E_{a,des}}{R \cdot T}\right) \quad (8)$$

$$E_{a,des} = E_{a,des}^0 - \beta_{des} \cdot \left(\frac{q_{CO_2}}{q_{max}}\right) \quad (9)$$

$$k_{des} = k_{des}^1 \cdot \exp\left(-\frac{\left(-\beta_{des} \cdot \frac{q_{CO_2}}{q_{max}}\right)}{R \cdot T}\right) \quad (10)$$

The equilibrium isotherm for CO₂ adsorption on K-HDMO was modelled with the empirical Freundlich equation for heterogeneous surfaces (Eq. 11).

$$q_{CO_2}^{eq} = k_{Fr} \cdot p_{CO_2}^{\frac{1}{n_{Fr}}} \quad (11)$$

2.7 Model parameters

The SEWGS model comprises a set of various parameters and properties, which have to be defined,

measured or calculated: Axial dispersion coefficients were determined according to Eq. 12 (Guffanti et al., 2021). Linear driving force approximation coefficients resulted from Eq. 13 (Yang, 1987). Gas mixture diffusion coefficients and effective diffusion coefficients were taken from (Poling et al., 2020).

$$D_{ax,i} = D_{mix,i} \cdot \sqrt{\varepsilon_b} + u \cdot r_p \quad (12)$$

$$k_{LDF,i} = \frac{15 \cdot D_{eff,i}}{r_p^2} \quad (13)$$

Kinetic and sorption isotherm parameters were obtained through nonlinear least-squares regression by minimization of the objective function (Eq. 14). Optimized parameters contained in ϕ were computed in MATLAB by the optimization solver `lsqnonlin`.

$$F(\phi) = \sum \left(\frac{y_{sim}(\phi) - y_{exp}}{y_{sim}(\phi)} \right)^2 \quad (14)$$

Table 2 gives an overview of all required information concerning the operating conditions in the simulation base case.

2.8 Numerical solution

A novel graphical implementation approach was applied for solving the set of partial differential and algebraic equations simultaneously in all six reaction chambers in the MATLAB Simulink programming environment (Figure 3). The implementation is based on the Method-of-Lines with uniform spatial discretization in up to 100 finite differences. It employs the built-in solver `ode23t` for moderately stiff ordinary differential equations. The cyclic PSA operation was performed by a state-machine created in the Simulink add-on Stateflow. This state-machine switches the PSA modes by leveraging discrete valve positions just like in the real plant. Switches from reactive adsorption to regeneration during runtime can, for example, be triggered by a predefined threshold of CO₂ in the product gas. Detailed information on the implementation method and numerical solution of the hybrid model can be found in our recent publication (Stadler et al., 2022b).

TABLE 1 Reactor model equations for bulk and particle phase.

Bulk gas phase	$\varepsilon_b \frac{\partial c_i}{\partial t} = -u \frac{\partial c_i}{\partial z} + \varepsilon_b D_{ax,i} \frac{\partial^2 c_i}{\partial z^2} + (1 - \varepsilon_b) k_{LDF,i} (\bar{c}_i - c_i)$	(15)
Particle void phase	$\varepsilon_p \frac{\partial \bar{c}_i}{\partial t} = \varepsilon_p k_{LDF,i} (c_i - \bar{c}_i) + w_{cat} \rho \nu_i r_{WGS} - (1 - w_{cat}) \rho a_{ads/des,i}$	(16)
Particle solid phase	$\frac{\partial q_{CO_2}}{\partial t} = a_{ads/des,CO_2}$	(17)

$i = CO, H_2O, CO_2, H_2, N_2$. $\nu_i = -1$ for $i = CO, H_2O$; $\nu_i = 1$ for $i = CO_2, H_2$; $\nu_i = 0$ for $i = N_2$. $a_{ads/des,i} = 0$ for $i = CO, H_2O, H_2, N_2$; $a_{ads/des,i} = \text{Eq. 6/Eq. 7}$ for $i = CO_2$.

TABLE 2 Parameters and operating conditions used in the pilot plant base case simulation.

Reactor dimensions		
Number of chambers		6
Number of slits per chamber		7
Rectangular slit dimensions		4 mm × 50 mm × 300 mm
General parameters		
Bed void fraction	ϵ_b	0.4
Particle void fraction	ϵ_p	0.5
Bulk density	ρ	1,096 kg m ⁻³
Particle radius	r_p	100 μ m
Catalyst weight fraction ^a	w_{cat}	0.05
Adsorption parameters		
Pressure	p	8 bar
Temperature	T	250°C
Flow rate	F_{STP}	1,000 ml min ⁻¹
CO volume fraction	$y_{CO,feed}$	0.3
H ₂ O volume fraction	$y_{H_2O,feed}$	0.6
N ₂ volume fraction	$y_{N_2,feed}$	0.1
Desorption parameters		
Pressure	p	1 bar
Temperature	T	250°C
Flow rate	F_{STP}	500 ml min ⁻¹
H ₂ O volume fraction	$y_{H_2O,feed}$	0.4
N ₂ volume fraction	$y_{N_2,feed}$	0.6

^aCatalyst is homogeneously mixed with sorbent in the first quarter of the reactor length.

3 Results and discussion

3.1 Water-gas shift catalyst activity

The empirical WGS reaction rate expression (Eq. 4) adequately described the catalyst's behavior under the prevailing conditions in the SEWGS system. Experimental CO conversion rates for three different temperatures are shown together with fitted model data in Figure 4. The fitted kinetic parameters are listed in Table 3. The values for the frequency factor as well as the activation energy are comparable to those presented in literature for resembling catalysts, albeit, slightly lower conversions were obtained (Choi and Stenger, 2003; Smirniotis, 2015).

3.2 CO₂ sorption on K-HDMO

The Freundlich adsorption equation (Eq. 11) provided a good fit for the measured CO₂ equilibrium isotherm on K-HDMO at 250°C under dry conditions (Figure 5). The empirical correlation

was capable to account for the heterogeneity of the sorbent's surface (Al-Ghouthi and Da'ana, 2020). It required the definition of the temperature-dependent adsorption intensity, which is an indicator for the adsorption strength, and the Freundlich coefficient, which is related to the adsorption capacity (Dada et al., 2012). As $1/n_{Fr}$ is smaller than one, normal adsorption can be assumed. The fitted parameters are listed in Table 3. The CO₂ uptake of the self-prepared sorbent was relatively low compared to resembling sorbents reported in literature, where adsorption capacities ranging from 0.1 mmol g⁻¹ to 1 mmol g⁻¹ can be found (Iruetagoiena Ferrer, 2016).

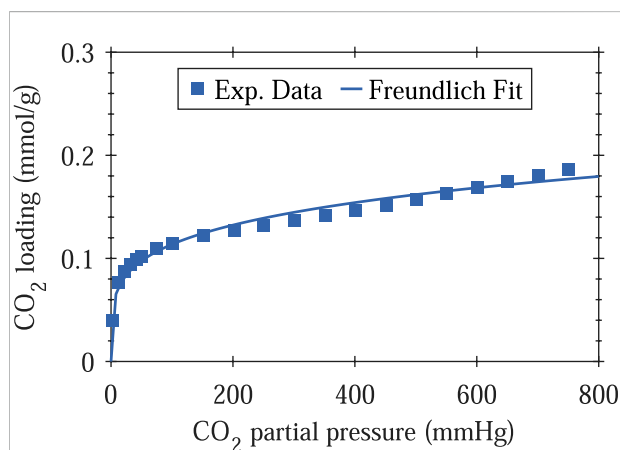
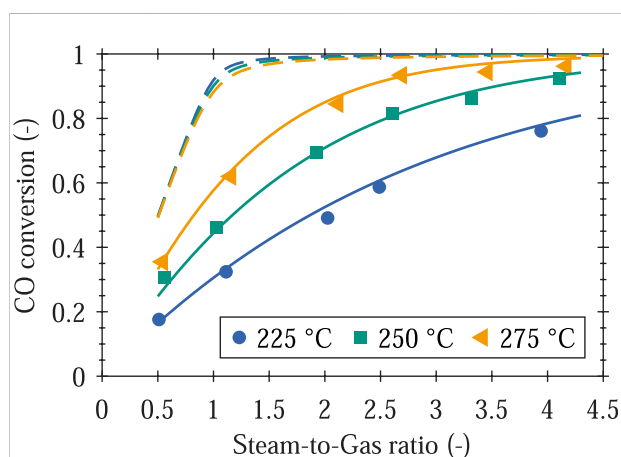
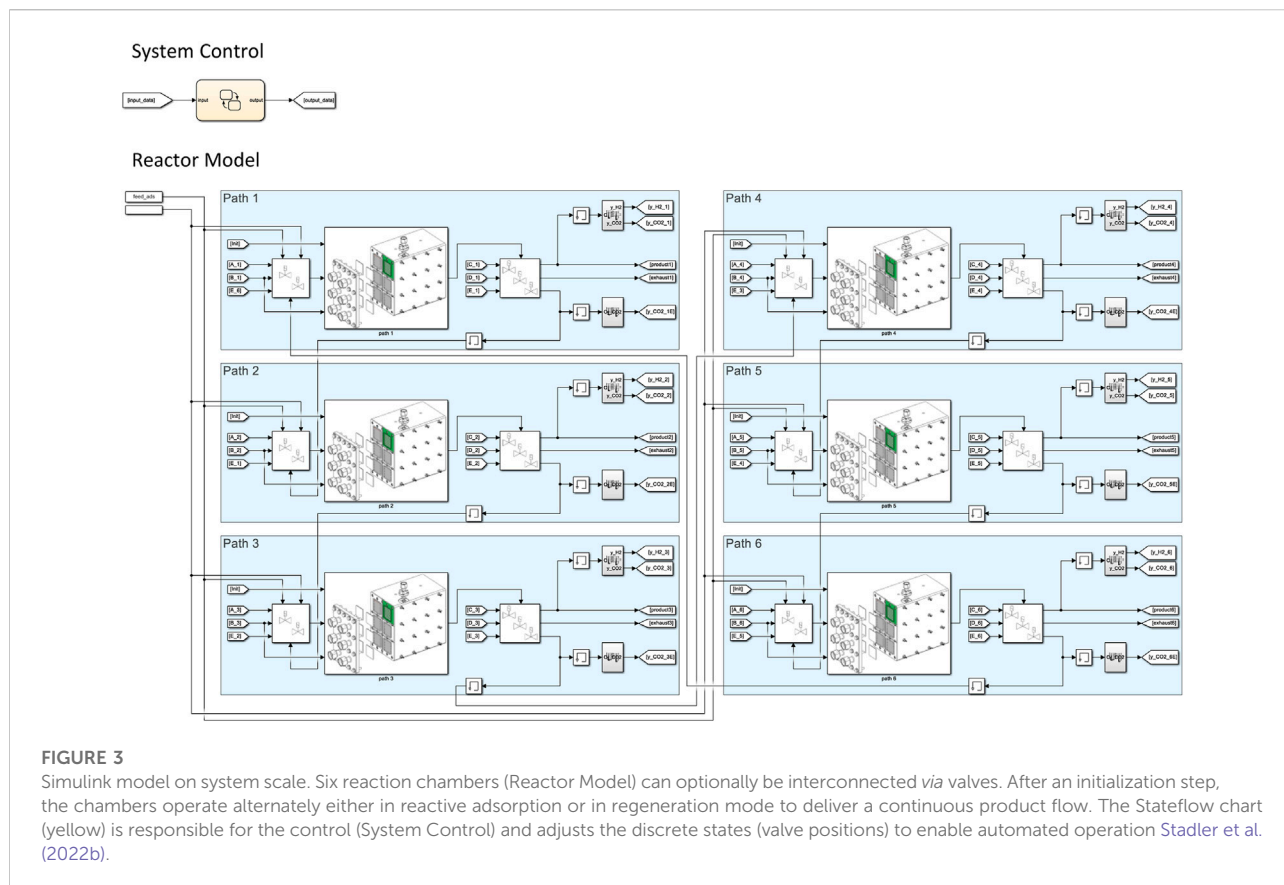
3.3 Breakthrough experiments

The breakthrough experiments in the single reaction chamber PBMR revealed an appropriate stability and cyclic working capacity for the tested PSA conditions.

In Figure 6, the first five cycles of an experimental run with pure K-HDMO filling are shown. Non-adsorbing CO was co-fed for comparison with adsorbing CO₂, and the time shift between the evolution of the gases indicated CO₂ adsorption on K-HDMO. After the first cycle, a significant loss of sorption capacity was observed. Due to severe back-mixing in the tubes and in other parts downstream the reactor, no sharp ramp, as expected for ideal plug-flow behavior, was detectable. Therefore, the residence time distribution for the employed reactor had to be considered for quantitative claims.

Experimental results for a long-term run with catalyst-sorbent-mixture filling are presented in Figure 7. Back-mixing and residence time distribution also had an apparent effect on the breakthrough curves here. It has been proven that long-term operation up to at least 70 cycles was possible (depicted are the curves for cycle 1, 3, 13, 43, 63). A constant steady-state CO conversion of 89.6% was reached, and the time shift between H₂ and CO₂ changed less than 20% over 70 cycles. During desorption (cycle 2 to cycle 70), a relatively constant value of (0.011 ± 0.002) mmol_{CO₂} g⁻¹ was released from the sorbent.

A computational approach was applied to estimate the kinetic parameters proposed in the model in Section 2.6. Blank experiments were implemented to account for the residence time distribution of the gas flow in the overall setup to get a set of appropriate parameters which best fit the experimental data for the tested process conditions. To account for the significant drop in sorption capacity due to irreversible bulk carbonate formation, the first cycle was not considered for the parameter estimation. The maximum sorbent loading was required to express the dependence of the desorption rate from the surface coverage (Eq. 10) and was calculated for a pressure of 20 bar, as also done by others (Coenen et al., 2019). Experimental and modelled curves are shown together in Figure 8 for the third cycle on K-HDMO without (Figure 8A) and with catalyst (Figure 8B) for a feed consisting of 5% CO and



20% H₂O, balanced in N₂. It can be seen that the initial increase is fitted quite well, while the experimental and simulated CO curves in the upper part deviate when approaching the final state.

TABLE 3 Kinetic and equilibrium parameters obtained by nonlinear regression from experimental data.

WGS reaction rate parameters	
k_{CO}	$2.01 \times 10^5 \text{ mol bar}^{-2} \text{ g}^{-1} \text{ h}^{-1}$
E_a	$51.845 \text{ kJ mol}^{-1}$
Isotherm parameters	
k_{Fr}	$0.177 \text{ mmol g}^{-1} \text{ bar}^{-n_{\text{Fr}}}$
$1/n_{\text{Fr}}$	0.220
Sorption kinetic parameters	
k_{ads}	0.1125 s^{-1}
k_{des}^1	$5.38 \times 10^{-4} \text{ s}^{-1}$
β_{des}	$74,000 \text{ J mol}^{-1}$

The set of kinetic parameters obtained by non-linear regression over a series of experiments is listed in Table 3. This model calibration can be used for simplified SEWGS simulation and is only valid for the tested conditions and materials. Simplifying assumptions had to be made due to experimental limitations. More elaborated models should additionally account for the highly important interactions of steam with the sorbent to describe the competitive adsorption of CO_2 and H_2O on K-HDMO (Coenen et al., 2019; Sebastiani et al., 2021). Therefore, an enhanced multi-component isotherm, as suggested by Boon et al. (2014) is required. Furthermore, a smaller setup with less pronounced influence of residence time distribution could lead to more precise data. Further experiments at different temperatures may be performed to further validate and refine the estimated model parameters.

However, the simplified parameterized model presented here served as a sufficient base considering setup and simulation times. The dynamic simulations on system scale can be used to determine real plant operating conditions.

3.4 Dynamic simulation

The dynamic MATLAB Simulink model on system scale enabled insights into every axial position of every reaction chamber of the pilot plant reactor at every time step. Due to automated switching between different modes during runtime, the influence of key operating parameters and design configurations on the overall process performance could be investigated.

Figure 9 presents MATLAB Simulink results for the pilot plant base case simulation in single stage configuration (Figures 9A,C,E) and serial (Figures 9B,D,F) configuration. The switch from M2 to M4 (single stage configuration) or M3 (serial configuration), respectively, was triggered as soon as the CO_2 fraction at the outlet of the reaction chamber exceeded $y_{\text{CO}_2} > 0.05$. Thus, the product purity in both cases was comparable. The switch from M3 to M4 in serial configuration occurred when $y_{\text{CO}_2} > 0.15$ for the gas being fed to the subsequent chamber. The operating schedules depicted in Figures 9A,B demonstrate that both configurations enabled the generation of high pressure H_2 in a single unit operation. As always at least one reaction chamber was in M2, continuous H_2 production was realized while the CO_2 content in the product was always kept below 5%. Cyclic studies exhibited that the process reached cyclic steady-state behavior within the first four operating cycles, what is well in line with previously published observations (Karagöz et al., 2019). The time spans of each operation mode (in Figures 9C,D

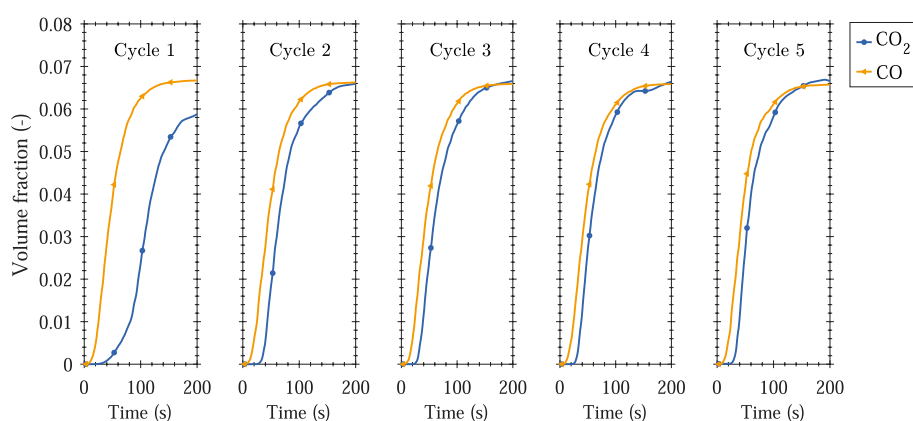


FIGURE 6

Experimental breakthrough curves (dry volume fraction) of CO_2 and CO for the first five adsorption cycles on pure K-HDMO sorbent (no catalyst). CO is shown for comparison. Sorbent mass: 9.70 g, temperature: 250°C , pressure: 8 bar, feed composition: 0.05/0.05/0.05/0.2/0.65 $\text{CO}_2/\text{H}_2/\text{H}_2\text{O}/\text{N}_2$. Regeneration pressure: 1 bar, regeneration feed composition: 0.4/0.6 $\text{H}_2\text{O}/\text{N}_2$.

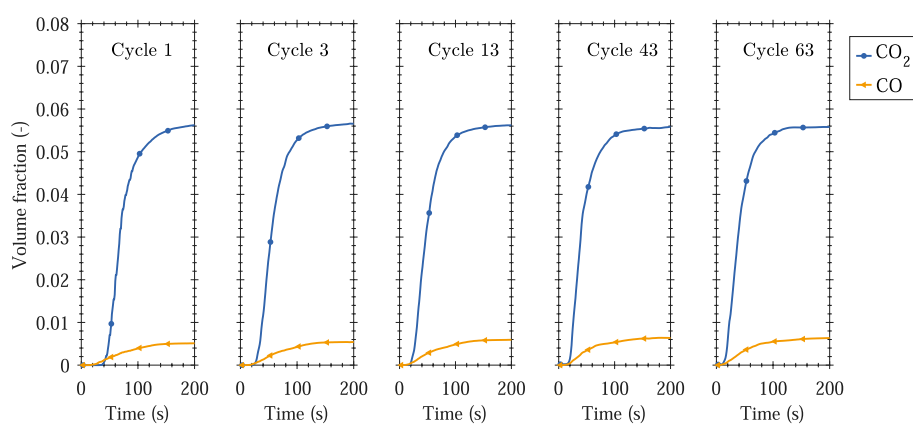


FIGURE 7

Experimental breakthrough curves (dry volume fraction) of CO₂ and CO for adsorption cycles 1, 3, 13, 43, and 63 on K-HDMO sorbent and Cu/ZnO/Al₂O₃ catalyst. Sorbent mass: 9.35 g, catalyst mass: 0.51 g, temperature: 250°C, pressure: 8 bar, feed composition: 0.05/0.2/0.75 CO/H₂O/N₂. Regeneration pressure: 1 bar, regeneration feed composition: 0.4/0.6 H₂O/N₂. Catalyst is homogeneously mixed with sorbent material in the first quarter of the reactor.

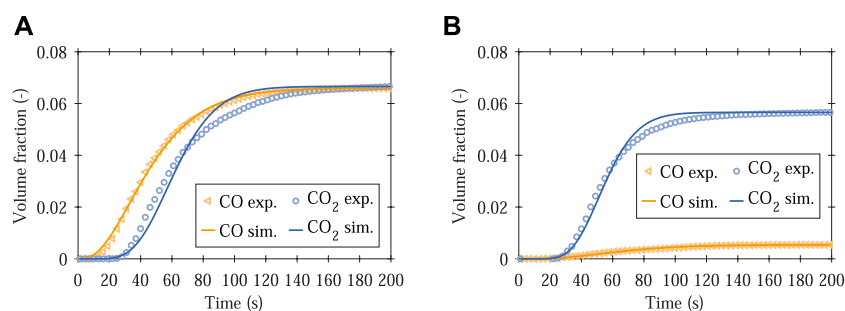


FIGURE 8

Exemplary experimental and simulated breakthrough curves. (A) third cycle on pure K-HDMO sorbent (see Figure 6), (B) third cycle on K-HDMO sorbent and Cu/ZnO/Al₂O₃ catalyst (see Figure 7).

shown for the first five cycles in chamber 1) did not change anymore after cycle 4. The relative sorbent loadings at the end of each operation mode based on the maximum loading (determined after 600 s reactive adsorption) are depicted in Figures 9E,F for the first five cycles in chamber 1. Owing to the serial configuration, the sorbent loading in each cycle could be increased by 7% compared to single stage configuration. Thus, interconnected reactor chambers in serial configuration can improve the overall performance of the process operation.

Figure 10 illustrates the CO₂ loading at the end of each reactive adsorption mode in serial configuration for the fifth cycle in chamber 1 over the reactor chamber length. Cycle 5 has an exemplary significance as the system already attained its long-term behavior by then. Chamber 1 was arbitrarily chosen and could be replaced by every other chamber, too. In both cases,

Figures 10A,B, the switch from M2 to M3 was triggered as soon as the CO₂ fraction in the product gas at the outlet of the reaction chamber reached $y_{\text{CO}_2} > 0.05$. The switch from M3 to M4 occurred when the CO₂ volume fraction to the subsequent chamber was $y_{\text{CO}_2} > 0.10$ (Figure 10A), or $y_{\text{CO}_2} > 0.15$ (Figure 10B). The larger area at the end of M3 in Figure 10B compared to Figure 10A shows that the K-HDMO loading could notably be improved with increasing M3-M4 threshold. Consequently, higher sorbent loadings could be realized resulting in longer cycle time spans and better efficiencies.

The influence of the M2-M4 threshold (in single stage configuration) is depicted in Figure 11. This key operating parameter controlled the switch from reactive adsorption to desorption and thereby, the purity of the product gas. The

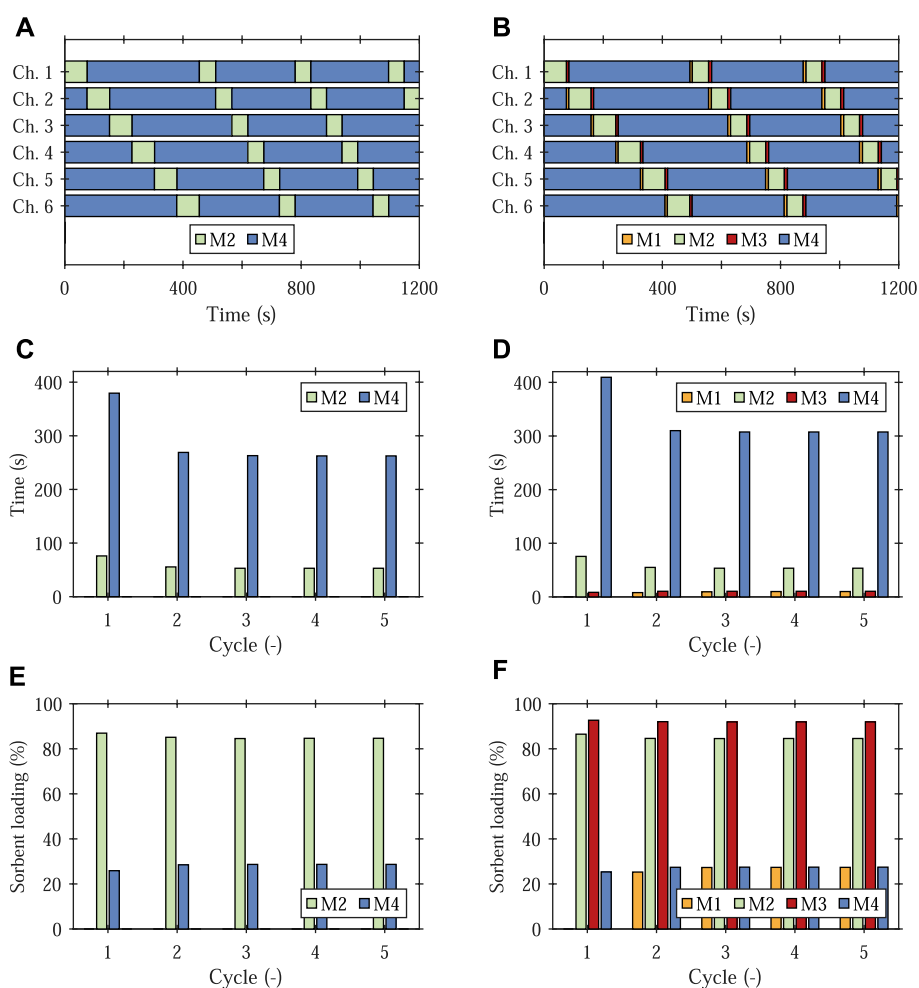


FIGURE 9

MATLAB Simulink results for the pilot plant base case simulation in single stage configuration (A,C,E) and serial configuration (B,D,F). The switch from M2 to M4 (single stage configuration) or M3 (serial configuration), respectively, is triggered as soon as $y_{(\text{CO}_2)} > 0.05$ in the outlet of the reaction chamber. The switch from M3 to M4 in serial configuration occurs when the CO_2 volume fraction to the subsequent chamber is $y_{(\text{CO}_2)} > 0.15$. (A,B) Operating schedule for all six reaction chambers, (C,D) Time span of each operation mode for the first five cycles in chamber 1, (E,F) Relative sorbent loading at the end of each operation mode for the first five cycles in chamber 1.

time span of M2 as well as the relative sorbent loading at the end of M2 increased with increasing M2-M4 threshold (Figure 11A). The latter observation is illustrated in terms of the CO_2 loading over the reactor length for various M2-M4 thresholds in Figure 11B. Here, it becomes apparent that the highest potential for intensified sorbent loading is given in the last third of the reactor length.

Another key operating parameter was found to be the adsorption-to-desorption flow ratio. With increasing adsorption flow, the time span of M2 as well as the sorbent loading at the end of M2 decreased (Figure 12A). However, the fraction of H_2 in the product gas remained constant and the product flow increased linearly with increasing feed. The sorbent loading over the whole reactor length was remarkably influenced

by the flow ratio (Figure 12B). Thus, a trade-off between reasonably high product flows and adequate sorbent loadings must be made to achieve acceptable switching times and process efficiencies. A less pronounced influence on the system behavior has been detected for the catalyst weight fraction. This parameter was varied from 0.02 to 0.08 and no remarkable effect on neither time span, sorbent loading nor H_2 production was observed.

Based on this case study performed with the novel simulation approach, important insights regarding the planned pilot plant operation and control could be gained by simulation-driven process design. Fast switching times and low sorbent loadings should be avoided in the compact pilot plant reactor to increase the process' efficiency and improve its overall performance.

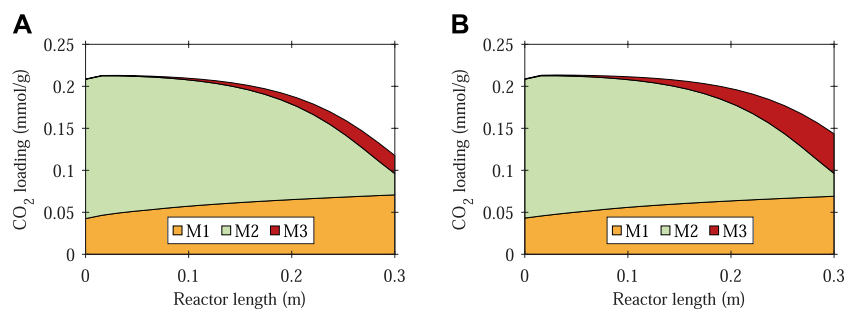


FIGURE 10 MATLAB Simulink results for the pilot plant base case simulation in serial configuration. CO₂ loading at the end of each reactive adsorption mode for cycle 5 in chamber 1 over the reactor length. The switch from M2 to M3 is triggered as soon as $y_{(\text{CO}_2)} > 0.05$ at the outlet of the reaction chamber. The switch from M3 to M4 occurs when the CO₂ volume fraction to the subsequent chamber is (A) $y_{(\text{CO}_2)} > 0.10$, (B) $y_{(\text{CO}_2)} > 0.15$.

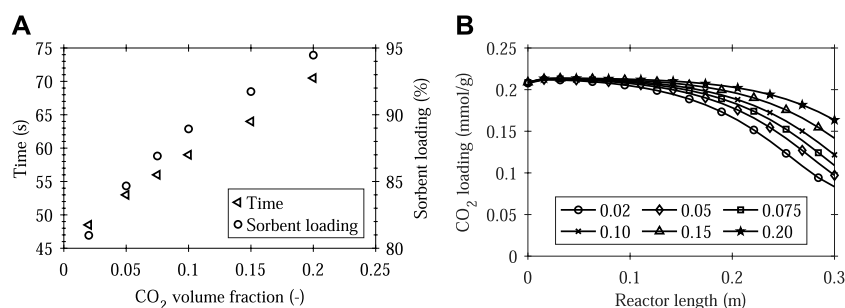


FIGURE 11 MATLAB Simulink results for the pilot plant base case simulation with various $y_{(\text{CO}_2)}$ thresholds (switch M2 to M4) in single stage configuration. (A) Time span of M2, and relative sorbent loading at the end of M2 as a function of the threshold CO₂ volume fraction (cycle 5 in chamber 1), (B) CO₂ loading at the end of M2 over the reactor length for various CO₂ volume fraction thresholds (cycle 5 in chamber 1).

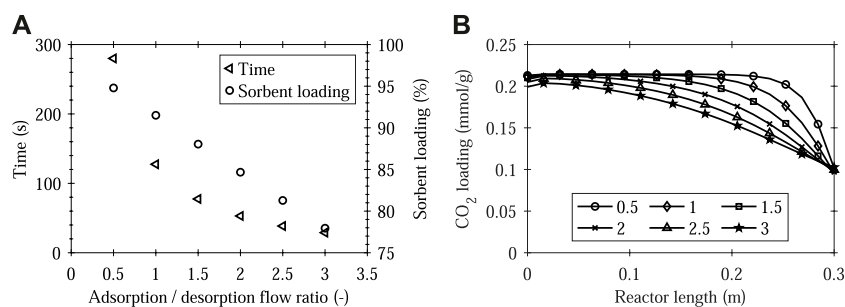


FIGURE 12 MATLAB Simulink results for the pilot plant base case simulation with various adsorption-to-desorption flow ratios in single stage configuration. The switch from M2 to M4 is triggered as soon as $y_{(\text{CO}_2)} > 0.05$ in the outlet of the reaction chamber. (A) Time span of M2, and relative sorbent loading at the end of M2 as a function of the adsorption-to-desorption flow ratio (cycle 5 in chamber 1), (B) CO₂ loading at the end of M2 over the reactor length for various adsorption-to-desorption ratios (cycle 5 in chamber 1).

4 Conclusion

A novel compact SEWGS reactor has been designed and built. It produces synthesis gas ($\text{CO} + \text{H}_2$) from pure CO in an advanced e-fuels process route. The overall process is currently demonstrated in a pilot plant. Simulation-driven process design was applied to determine optimized operation procedures for the intended reactor operation. Therefore, a comprehensive MATLAB Simulink model on system scale was developed. It is based on a reactor scale model accounting for simultaneous WGS reaction and CO_2 adsorption as well as consecutive desorption. It employs an empirical rate expression for the WGS reaction rate and the Freundlich isotherm model for CO_2 adsorption equilibrium. The kinetic and equilibrium parameters were fitted to experimental data obtained in laboratory-scale experiments and adequately described the process. The dynamic system scale model was used to quantify the influence of design configurations and key operating process parameters. The simulation case study revealed rapid convergence to a final periodic solution after the fourth cycle and continuous product generation. It was shown that the serial configuration with interconnected reaction chambers lead to intensified sorbent loading compared to simple single stage operation by 7%. Hence, better efficiencies could be realized due to longer cycle times. Investigations in single stage configuration exhibited a trade-off between high throughput (high adsorption flow) and high product purity (low M2-M4 threshold) which considerably determined the length of the switching times and the degree of the sorbent loading. Consequently, the dynamic simulation provided process guidelines for practical application to maximize switching time spans and sorbent loadings. It enabled valuable insights on how to operate the compact pilot plant reactor as efficient as possible with improved overall performance.

Data availability statement

The original contributions presented in the study are included in the article, further inquiries can be directed to the corresponding author.

References

- Al-Ghouthi, M. A., and Da'ana, D. A. (2020). Guidelines for the use and interpretation of adsorption isotherm models: A review. *J. Hazard. Mater.* 393, 122383. doi:10.1016/j.jhazmat.2020.122383
- Amadeo, N., and Laborde, M. (1995). Hydrogen production from the low-temperature water-gas shift reaction: Kinetics and simulation of the industrial reactor. *Int. J. Hydrogen Energy* 20, 949–956. doi:10.1016/0360-3199(94)00130-R
- Beaver, M. G., Caram, H. S., and Sircar, S. (2009). Selection of CO_2 chemisorbent for fuel-cell grade H_2 production by sorption-enhanced water

Author contributions

TS conducted the conception and design of the study, performed the simulations and data analysis, and wrote the first draft of the manuscript. LB and TS carried out the experiments. PP was responsible for the conceptual design of the research project. All authors contributed to manuscript revision, read, and approved the submitted version.

Funding

The work presented in this paper is part of the European project Kerogreen, which has received funding from the European Union's Horizon 2020 research and innovation programme under grant agreement No. 763909.

Acknowledgments

The authors kindly acknowledge the donation of sorbent material from Sasol GmbH, Germany. The authors would like to thank Kerstin Albers (Institut für Chemieingenieurwesen, Universität Ulm) for conducting CO_2 chemisorption measurements. TS kindly acknowledges financial support from the Joint Programme on Energy Storage of the European Energy Research Alliance for this publication.

Conflict of interest

The authors declare that the research was conducted in the absence of any commercial or financial relationships that could be construed as a potential conflict of interest.

Publisher's note

All claims expressed in this article are solely those of the authors and do not necessarily represent those of their affiliated organizations, or those of the publisher, the editors and the reviewers. Any product that may be evaluated in this article, or claim that may be made by its manufacturer, is not guaranteed or endorsed by the publisher.

gas shift reaction. *Int. J. Hydrogen Energy* 34, 2972–2978. doi:10.1016/j.ijhydene.2009.01.065

Bhagiyalakshmi, M., Lee, J. Y., and Jang, H. T. (2010). Synthesis of mesoporous magnesium oxide: Its application to CO_2 chemisorption. *Int. J. Greenh. Gas Control* 4, 51–56. doi:10.1016/j.ijggc.2009.08.001

Boon, J., Cobden, P. D., van Dijk, H., Hoogland, C., van Selow, E. R., and van Sint Annaland, M. (2014). Isotherm model for high-temperature, high-pressure adsorption of and on K-promoted hydrotalcite. *Chem. Eng. J.* 248, 406–414. doi:10.1016/j.cej.2014.03.056

- Boon, J., Cobden, P. D., van Dijk, H., and van Sint Annaland, M. (2015). High-temperature pressure swing adsorption cycle design for sorption-enhanced water-gas shift. *Chem. Eng. Sci.* 122, 219–231. doi:10.1016/j.ces.2014.09.034
- Choi, W. K., Kwon, T. I., Yeo, Y. K., Lee, H., Song, H. K., and Na, B. K. (2003). Optimal operation of the pressure swing adsorption (PSA) process for CO₂ recovery. *Korean J. Chem. Eng.* 20, 617–623. doi:10.1007/BF02706897
- Choi, Y., and Stenger, H. G. (2003). Water gas shift reaction kinetics and reactor modeling for fuel cell grade hydrogen. *J. Power Sources* 124, 432–439. doi:10.1016/S0378-7753(03)00614-1
- Coenen, K., Gallucci, F., Hensen, E., and van Sint Annaland, M. (2019). Kinetic model for adsorption and desorption of H₂O and CO₂ on hydrotalcite-based adsorbents. *Chem. Eng. J.* 355, 520–531. doi:10.1016/j.cej.2018.08.175
- Cunha, A. F., Moreira, M. N., Mafalda Ribeiro, A., Ferreira, A. P., Loureiro, J. M., and Rodrigues, A. E. (2015). How to overcome the water-gas-shift equilibrium using a conventional nickel reformer catalyst. *Energy Technol.* 3, 1205–1216. doi:10.1002/ente.201500175
- Cunha, A. F., Moreira, M. N., Ribeiro, A. M., Loureiro, J. M., Rodrigues, A. E., Terzan, J., et al. (2017). Synthesis gas adjustment by low temperature sorption enhanced water-gas shift reaction through a copper-zeolite 13X hybrid material. *Chem. Eng. Process. Process Intensif.* 121, 97–110. doi:10.1016/j.cep.2017.07.023
- Dada, A., Olalekan, A., Olatunya, A., and Dada, O. (2012). Langmuir, Freundlich, temkin and dubinin–radushkevich isotherms studies of equilibrium sorption of Zn 2+ unto phosphoric acid modified rice husk. *IOSR J. Appl. Chem.* 3, 38–45. doi:10.9790/5736-0313845
- Du, H., Williams, C. T., Ebner, A. D., and Ritter, J. A. (2010). *In situ* FTIR spectroscopic analysis of carbonate transformations during adsorption and desorption of CO₂ in K-promoted HTlc. *Chem. Mat.* 22, 3519–3526. doi:10.1021/cm100703e
- Faria, A. C., Trujillano, R., Rives, V., Miguel, C. V., Rodrigues, A. E., and Madeira, L. M. (2022). Alkali metal (Na, Cs and K) promoted hydrotalcites for high temperature CO₂ capture from flue gas in cyclic adsorption processes. *Chem. Eng. J.* 427, 131502. doi:10.1016/j.cej.2021.131502
- Fleming, G., and de Lépinay, I. (2019). *Environmental trends in aviation to 2050. ICAO Environmental Report* Chapter 1.
- Glud, W., Keller, K., Schönfelder, R., and Klemm, W. (1931). *Production of hydrogen*. US Patent US1816523.
- Goede, A. P. H. (2018). CO₂ neutral fuels. *EPJ Web Conf.* 189, 00010. doi:10.1051/epjconf/201818900010
- Guffanti, S., Visconti, C. G., van Kampen, J., Boon, J., and Groppi, G. (2021). Reactor modelling and design for sorption enhanced dimethyl ether synthesis. *Chem. Eng. J.* 404, 126573. doi:10.1016/j.cej.2020.126573
- Halabi, M. H., de Croon, M., van der Schaaf, J., Cobden, P. D., and Schouten, J. C. (2012). High capacity potassium-promoted hydrotalcite for CO₂ capture in H₂ production. *Int. J. Hydrogen Energy* 37, 4516–4525. doi:10.1016/j.ijhydene.2011.12.003
- Ho, Y. S. (2006). Review of second-order models for adsorption systems. *J. Hazard. Mater.* 136, 681–689. doi:10.1016/j.jhazmat.2005.12.043
- Hu, Y., Liu, W., Yang, Y., Qu, M., and Li, H. (2019). CO₂ capture by Li₄SiO₄ sorbents and their applications: Current developments and new trends. *Chem. Eng. J.* 359, 604–625. doi:10.1016/j.cej.2018.11.128
- IATA (2020). Recovery delayed as international travel remains locked down. Available at: <https://www.iata.org/en/pressroom/pr/2020-07-28-02/> (Accessed June 14, 2022).
- IPCC (2018). *Global Warming of 1.5°C. An IPCC Special Report on the impacts of global warming of 1.5°C above pre-industrial levels and related global greenhouse gas emission pathways, in the context of strengthening the global response to the threat of climate change, sustainable development, and efforts to eradicate poverty*. Cambridge, UK and New York, NY, USA: Cambridge University Press. doi:10.1017/9781009157940
- Iruetagoiena Ferrer, D. (2016). *Supported layered double hydroxides as CO₂ adsorbents for sorption-enhanced H₂ production*. Cham: Springer International Publishing. doi:10.1007/978-3-319-41276-4
- Iwan, A., Stephenson, H., Ketchie, W. C., and Lapkin, A. A. (2009). High temperature sequestration of CO₂ using lithium zirconates. *Chem. Eng. J.* 146, 249–258. doi:10.1016/j.cej.2008.06.006
- Jansen, D., van Selow, E., Cobden, P., Manzolini, G., Macchi, E., Gazzani, M., et al. (2013). SEWGS technology is now ready for scale-up! *Energy Procedia* 37, 2265–2273. doi:10.1016/j.egypro.2013.06.107
- Karagöz, S., Chen, H., Cao, M., Tsotsis, T. T., and Manousiouthakis, V. I. (2019). Multiscale model based design of an energy-intensified novel adsorptive reactor process for the water gas shift reaction. *AIChE J.* 65, e16608. doi:10.1002/aic.16608
- Kerogreen (2022). KEROGREEN – towards sustainable and green aviation fuel production. Available at: <https://www.kerogreen.eu/> (Accessed June 14, 2022).
- Kirsch, H., Brübach, L., Loewert, M., Riedinger, M., Gräfenhahn, A., Böltken, T., et al. (2020). CO₂-neutrale Fischer–Tropsch–Kraftstoffe aus dezentralen modularen Anlagen: Status und Perspektiven. *Chem. Ing. Tech.* 92, 91–99. doi:10.1002/cite.201900120
- Koryabkina, N., Phatak, A., Ruettinger, W., and Farrauto, R. R. F. (2003). Determination of kinetic parameters for the water-gas shift reaction on copper catalysts under realistic conditions for fuel cell applications. *J. Catal.* 217, 233. doi:10.1016/S0021-9517(03)00050-2
- Lee, D. S., Fahey, D. W., Skowron, A., Allen, M. R., Burkhardt, U., Chen, Q., et al. (2021). The contribution of global aviation to anthropogenic climate forcing for 2000 to 2018. *Atmos. Environ.* 244, 117834. doi:10.1016/j.atmosenv.2020.117834
- Lee, J. M., Min, Y. J., Lee, K. B., Jeon, S. G., Na, J. G., and Ryu, H. J. (2010). Enhancement of CO₂ sorption uptake on hydrotalcite by impregnation with K₂CO₃. *Langmuir* 26, 18788–18797. doi:10.1021/la102974s
- Lee, K. B., Beaver, M. G., Caram, H. S., and Sircar, S. (2008). Effect of reaction temperature on the performance of thermal swing sorption-enhanced reaction process for simultaneous production of fuel-cell-grade H₂ and compressed CO₂ from synthesis gas. *Ind. Eng. Chem. Res.* 47, 6759–6764. doi:10.1021/ie071372k
- León, M., Díaz, E., Bennici, S., Vega, A., Ordóñez, S., and Auroux, A. (2010). Adsorption of CO₂ on hydrotalcite-derived mixed oxides: Sorption mechanisms and consequences for adsorption irreversibility. *Ind. Eng. Chem. Res.* 49, 3663–3671. doi:10.1021/ie902072a
- Li, Z., Liu, Y., and Cai, N. (2012). Effect of CaO hydration and carbonation on the hydrogen production from sorption enhanced water gas shift reaction. *Int. J. Hydrogen Energy* 37, 11227–11236. doi:10.1016/j.ijhydene.2012.04.160
- Martins, V., Miguel, C. V., Gonçalves, J. C., Rodrigues, A. E., and Madeira, L. M. (2022). Modeling of a cyclic sorption-desorption unit for continuous high temperature CO₂ capture from flue gas. *Chem. Eng. J.* 434, 134704. doi:10.1016/j.cej.2022.134704
- Millward, A. R., and Yaghi, O. M. (2005). Metal-organic frameworks with exceptionally high capacity for storage of carbon dioxide at room temperature. *J. Am. Chem. Soc.* 127, 17998–17999. doi:10.1021/ja057003z
- Moe, J. M. (1962). Design of water-gas shift reactors. *Chem. Eng. Prog.* 58, 3.
- Moreira, M. N., Ribeiro, A. M., Cunha, A. F., Rodrigues, A. E., Zabitskiy, M., Djinović, P., et al. (2016). Copper based materials for water-gas shift equilibrium displacement. *Appl. Catal. B Environ.* 189, 199–209. doi:10.1016/j.apcatb.2016.02.046
- Mulloth, L. M., and Finn, J. E. (1998). *Carbon dioxide adsorption on a 5A zeolite designed for CO₂ removal in spacecraft cabins*. Washington, DC, USA: National Aeronautics and Space Administration.
- Najmi, B., Bolland, O., and Colombo, K. E. (2016). A systematic approach to the modeling and simulation of a Sorption Enhanced Water Gas Shift (SEWGS) process for CO₂ capture. *Sep. Purif. Technol.* 157, 80–92. doi:10.1016/j.seppur.2015.11.013
- Oliveira, E. L., Grande, C. A., and Rodrigues, A. E. (2008). CO₂ sorption on hydrotalcite and alkali-modified (K and Cs) hydrotalcites at high temperatures. *Sep. Purif. Technol.* 62, 137–147. doi:10.1016/j.seppur.2008.01.011
- Ovesen, C. V., Clausen, B. S., Hammershøi, B. S., Steffensen, G., Askgaard, T., Chorkendorff, I., et al. (1996). A microkinetic analysis of the water-gas shift reaction under industrial conditions. *J. Catal.* 158, 170–180. doi:10.1006/jcat.1996.0016
- Petrescu, L., Chisalita, D. A., Cormos, C. C., Manzolini, G., Cobden, P., and van Dijk, H. (2019). Life cycle assessment of SEWGS technology applied to integrated steel plants. *Sustainability* 11, 1825. doi:10.3390/su11071825
- Poling, B. E., Prausnitz, J. M., and O'Connell, J. P. (2020). *Properties of gases and liquids*. Fifth Edition. New York, N.Y.: McGraw-Hill Education and McGraw Hill.
- Rives, V. (2002). Characterisation of layered double hydroxides and their decomposition products. *Mater. Chem. Phys.* 75, 19–25. doi:10.1016/S0254-0584(02)00024-X
- Salomé Macedo, M., Soria, M. A., and Madeira, L. M. (2021). High temperature CO₂ sorption using mixed oxides with different Mg/Al molar ratios and synthesis pH. *Chem. Eng. J.* 420, 129731. doi:10.1016/j.cej.2021.129731
- Sebastiani, F., James, J., van Dijk, H., Pieterse, J. A., Boon, J., Cobden, P. D., et al. (2021). Modelling of CO₂ and H₂O interaction during adsorption cycles on hydrotalcite for SEWGS applications. *SSRN J.* doi:10.2139/ssrn.3811608
- Sebastiani, F., Lucking, L., Sarić, M., James, J., Boon, J., van Dijk, H. J. A., et al. (2022). Steam and pressure management for the conversion of steelworks arising

- gases to H₂ with CO₂ capture by stepwise technology. *Separations* 9, 20. doi:10.3390/separations9010020
- Siriwardane, R. V., Shen, M. S., Fisher, E. P., and Poston, J. A. (2001). Adsorption of CO₂ on molecular sieves and activated carbon. *Energy Fuels* 15, 279–284. doi:10.1021/ef000241s
- Smirniotis, P. (2015). *Water gas shift reaction: Research developments and applications*. Burlington: Elsevier Science.
- Soria, M. A., Rocha, C., Tosti, S., Mendes, A., and Madeira, L. M. (2019). CO_x free hydrogen production through water-gas shift reaction in different hybrid multifunctional reactors. *Chem. Eng. J.* 356, 727–736. doi:10.1016/j.cej.2018.09.044
- Soria, M. A., Tosti, S., Mendes, A., and Madeira, L. M. (2015). Enhancing the low temperature water-gas shift reaction through a hybrid sorption-enhanced membrane reactor for high-purity hydrogen production. *Fuel* 159, 854–863. doi:10.1016/j.fuel.2015.07.035
- Stadler, T. J., Barbig, P., Kiehl, J., Schulz, R., Klövekorn, T., and Pfeifer, P. (2021). Sorption-enhanced water-gas shift reaction for synthesis gas production from pure CO: Investigation of sorption parameters and reactor configurations. *Energies* 14, 355. doi:10.3390/en14020355
- Stadler, T. J., Bertin-Mente, B., Dittmeyer, R., Brübach, L. T., Böltken, T., and Pfeifer, P. (2022a). Influence of CO₂-rich syngas on the selectivity to C10–C14 in a coupled Fischer–Tropsch/hydrocracking process. *Chem. Ing. Tech.* 94, 289–298. doi:10.1002/cite.202100172
- Stadler, T. J., Knoop, J. H., Decker, S., and Pfeifer, P. (2022b). Numerical simulation approach for a dynamically operated sorption-enhanced water-gas shift reactor. *Processes* 10, 1160. doi:10.3390/pr10061160
- Uchida, H., Isogai, N., Oba, M., and Hasegawa, T. (1967). The zinc oxide-copper catalyst for carbon monoxide-shift conversion. I. The dependency of the catalytic activity on the chemical composition of the catalyst. *Bull. Chem. Soc. Jpn.* 40, 1981–1986. doi:10.1246/bcsj.40.1981
- UNEP (2021). *Emissions Gap Report 2021: The Heat Is on - a world of climate promises not yet delivered*. Nairobi, Kenya: UNEP.
- van Selow, E. R., Cobden, P. D., van Dijk, H., Walspurger, S., Verbraeken, P. A., and Jansen, D. (2013). Qualification of the ALKASORB sorbent for the sorption-enhanced water-gas shift process. *Energy Procedia* 37, 180–189. doi:10.1016/j.egypro.2013.05.100
- van Selow, E. R., Cobden, P. D., Wright, A. D., van den Brink, R. W., and Jansen, D. (2011). Improved sorbent for the sorption-enhanced water-gas shift process. *Energy Procedia* 4, 1090–1095. doi:10.1016/j.egypro.2011.01.159
- Wang, S., Shen, H., Fan, S., Zhao, Y., Ma, X., and Gong, J. (2013). Enhanced CO₂ adsorption capacity and stability using CaO-based adsorbents treated by hydration. *AIChE J.* 59, 3586–3593. doi:10.1002/aic.14126
- Yang, R. T. (1987). “Gas separation by adsorption processes,” in *Butterworths series in chemical engineering* (Boston: Butterworths).
- Yin, G., Liu, Z., Liu, Q., and Wu, W. (2013). The role of different properties of activated carbon in CO₂ adsorption. *Chem. Eng. J.* 230, 133–140. doi:10.1016/j.cej.2013.06.085
- Yong, Z., Mata, V., and Rodrigues, A. E. (2001). Adsorption of carbon dioxide onto hydrotalcite-like compounds (HTLcs) at high temperatures. *Ind. Eng. Chem. Res.* 40, 204–209. doi:10.1021/ie000238w
- Zheng, Y., Shi, Y., Li, S., Yang, Y., and Cai, N. (2014). Elevated temperature hydrogen/carbon dioxide separation process simulation by integrating elementary reaction model of hydrotalcite adsorbent. *Int. J. Hydrogen Energy* 39, 3771–3779. doi:10.1016/j.ijhydene.2013.12.167
- Zhu, X., Li, S., Shi, Y., and Cai, N. (2019). Recent advances in elevated-temperature pressure swing adsorption for carbon capture and hydrogen production. *Prog. Energy Combust. Sci.* 75, 100784. doi:10.1016/j.peccs.2019.100784
- Zhu, X., Shi, Y., and Cai, N. (2017). High-pressure carbon dioxide adsorption kinetics of potassium-modified hydrotalcite at elevated temperature. *Fuel* 207, 579–590. doi:10.1016/j.fuel.2017.06.137

Nomenclature

Abbreviations

Ch. Chamber
FID Flame ionization detector
GC Gas chromatograph
HDMO Hydrotalcite-derived mixed oxide
HTC Hydrotalcite
K-HDMO Potassium-impregnated hydrotalcite-derived mixed oxide
K-HTC Potassium-impregnated hydrotalcite
LDF Linear driving force
M1-M4 Operation mode 1-4
PBMR Packed bed microchannel reactor
PGA Process gas analyzer
PSA Pressure swing adsorption
SAF Sustainable aviation fuel
SEWGS Sorption-enhanced water-gas shift
TCD Thermal conductivity detector
WGS Water-gas shift

Symbols

β_{des} activation energy change (J mol^{-1})
$\Delta H_{\text{R}}^{\ominus}$ standard reaction enthalpy (kJ mol^{-1})
ϵ_{b} bed void fraction (–)
ϵ_{p} particle void fraction (–)
ν_i stoichiometric reaction coefficient (–)
ρ bulk density (kg m^{-3})
$a_{\text{ads,des},i}$ adsorption/ desorption rate ($\text{mol kg}^{-1} \text{s}^{-1}$)
\bar{c}_i particle void phase concentration (mol m^{-3})
c_i bulk phase concentration (mol m^{-3})
$D_{\text{ax},i}$ axial dispersion coefficient ($\text{m}^2 \text{s}^{-1}$)

$D_{\text{eff},i}$ effective diffusion coefficient ($\text{m}^2 \text{s}^{-1}$)
$D_{\text{mix},i}$ gas mixture diffusion coefficient ($\text{m}^2 \text{s}^{-1}$)
E_{a} activation energy (J mol^{-1})
$E_{\text{a,des}}$ activation energy for desorption (J mol^{-1})
$E_{\text{a,des}}^0$ activation energy for desorption (J mol^{-1})
eq equilibrium (–)
exp experimental (–)
F objective function (–)
F_{STP} flow rate (ml min^{-1})
i species CO , H_2O , CO_2 , H_2 , N_2 (–)
k_{∞} frequency factor ($\text{mol bar}^{-2} \text{g}^{-1} \text{h}^{-1}$)
$k_{\text{ads/des}}$ adsorption/ desorption coefficient (s^{-1})
$k_{\text{des}}^{0/1}$ desorption coefficient (s^{-1})
K_{eq} WGS equilibrium constant (–)
k_{Fr} Freundlich constant ($\text{mmol g}^{-1} \text{bar}^{-n_{\text{Fr}}}$)
$k_{\text{LDF},i}$ linear driving force coefficient (s^{-1})
\dot{n}_i molar flow (mol s^{-1})
n_{Fr} Freundlich adsorption intensity (–)
$p_{(i)}$ (partial) pressure (bar)
$q_{\text{CO}_{2\{i\}}}$ CO_2 sorbent loading (mol kg^{-1})
q_{max} maximum CO_2 sorbent loading (mol kg^{-1})
R gas constant ($\text{J mol}^{-1} \text{K}^{-1}$)
r_{p} particle radius (m)
r_{WGS} WGS reaction rate ($\text{mol g}^{-1} \text{h}^{-1}$)
S/G steam-to-gas ratio (–)
sim simulation (–)
T temperature (K)
t time (s)
u gas velocity (m s^{-1})
w_{cat} catalyst weight fraction (–)
X_{CO} CO conversion (–)
y volume fraction (–)
z axial coordinate (m)